Chapter 6
Non-local Transport of Electrons in Plasmas

Abstract Since plasma is high temperature and the charge particles are running with high temperature, for example, at 1 keV, about the velocity of 10^9 (electron) and 2×10^7 (ion) [cm/s]. Since Coulomb mean-free-path is proportional to $(velocity)^4$, higher velocity component transfers its energy over a long distance without Coulomb collision. This is usually called as "non-local transport" and the traditional diffusion model in neutral gas cannot be applicable. In laser plasma, the locally heated electron thermal energy is transported into cold over-dense region non-locally. The best way to solve such problem is to solve Fokker-Planck equation, while it is time consuming and some theoretical models have been proposed and studied over the last four decades. The physics of such models are explained here and most recent model SNB is shown and compared to experiments. The difficulty of transport of charges particles such as electrons is how to include the effect of electrostatic field and magnetic field self-consistently.

6.1 Spitzer-Harm Diffusion Model

6.1.1 Model Equation for Diffusion

Consider a simple equation describing time evolution of temperature. Assume that the particles carry the energy of plasma proportional to the temperature T. The plasma particles, mainly electrons, are assumed to be in random walk over every time interval Δt. The probability of the displacement during the time interval Δx is given as the probability density W(Δx, Δt). Then, the time evolution of the distribution of the temperature T is governed by

$$T(x,t) = \int_{-\infty}^{\infty} W(\Delta x, \Delta t) T(x - \Delta x, t - \Delta t) d(\Delta x) \tag{6.1}$$

Note that for simplicity Δt is assumed constant.

Under the condition that the spatial variation of T is gentle enough, (6.1) can be approximated with Taylor expansion to reduce to the form.

H. Takabe, *The Physics of Laser Plasmas and Applications - Volume 2*,
Springer Series in Plasma Science and Technology,
https://doi.org/10.1007/978-3-031-45473-8_6

$$T(x-\Delta x, t-\Delta t) = T(x,t) - \Delta x \frac{\partial T}{\partial x} + \frac{1}{2}(\Delta x)^2 \frac{\partial^2 T}{\partial x^2} + \cdots \tag{6.2}$$

In (6.1), the **probability function** W(Δx, Δt) is normalized,

$$\int_{-\infty}^{\infty} W(\Delta x, \Delta t) d(\Delta x) = 1 \tag{6.3}$$

It is also reasonable to assume that W(Δx, Δt) is an even function of Δx.

Inserting (6.2) to (6.1), the following diffusion equation is obtained.

$$\begin{aligned} &\frac{\partial}{\partial t} T = \frac{\partial}{\partial x}\left(\chi \frac{\partial}{\partial x} T\right), \\ &\chi = \frac{1}{2\Delta t} \int_{-\infty}^{\infty} W(\Delta x)(\Delta x)^2 d(\Delta x) \\ &\chi = \frac{1}{2} v \Delta x \Rightarrow \chi \approx \frac{\left\langle (\Delta x)^2 \right\rangle}{\Delta t} \end{aligned} \tag{6.4}$$

where $< >$ represents the ensemble average and we assumed that the space integral of T should be conserved.

$$\int_{-\infty}^{\infty} T(x,t) dx = Q : const. \tag{6.5}$$

This diffusion approximation is valid only when the following condition is satisfied.

$$\left| \frac{\Delta x}{T} \frac{\partial T}{\partial x} \right| \equiv \frac{\Delta x}{L_T} < < 1 \tag{6.6}$$

where L_T is the scale length of the gradient of T.

Let us consider that (6.4) is the energy diffusion by electron motion in plasma, the heat flux by the electron thermal motion should be in the form.

$$q_e = \frac{3}{2} n_e \chi(T_e) \nabla T_e \approx n_e v_e \lambda_e \nabla T_e = q_{FS} \frac{\lambda_e}{L_T} \tag{6.7}$$

where $v_e = (T_e/m)^{1/2}$, λ_e is the electron average mean-free-path, and q_{FS} is the **free streaming heat flux** defined by

$$q_{FS} = n_e v_e T_e \tag{6.8}$$

The free-streaming heat flux is the maximum of the heat flux by all electron of Maxwell distribution in one–direction. If we integrate the heat flux it is 0.6 times the free streaming flux.

In a historical paper by Spitzer-Harm [1], the mathematical formula of the electron heat conduction in fully ionized plasma was derived by starting with Fokker-Planck equation as we see soon. Its mathematical form is derived from the above simple model. Since the mean-free-path has the following relation,

$$\lambda_e \propto \frac{T_e^2}{n_e} \tag{6.9}$$

The **Spitzer-Harm heat flux** q_{SH} is given from (6.4).

$$q_e \equiv q_{SH} = -\kappa_0 T_e^{5/2} \nabla T_e \tag{6.10}$$

where κ_0 is a constant. This heat flux is already shown in (2.109). The heat flux of (6.10) has been widely used to describe the electron energy transport.

6.1.2 Flux Limit

In the early time 1970s of laser plasma research, it was found that the flux (6.7) is limited by the maximum much less than (6.8) and so-called **flux limiter** is proposed an ad hock method to be installed in simulation codes [2]. The flux-limiter was widely used in hydrodynamic simulations, because the temperature of the laser heated region becomes low without the flux-limiter to give higher absorption rate of laser via classical absorption as suggested in Chap. 2 in Volume 1. In the case where the flux-limiter is adopted in the simulation code, the heat flux propagating to higher density region is limited and the electron temperature in the absorption region becomes higher, consequently the absorption rate is suppressed.

In laser produced plasmas, for example, it has been well recognized that a simple diffusive expression of electron transport given in (2.109) cannot be applicable. The phenomenon has been called **flux-limit**. In physics integrated computer simulation based on hydrodynamic description the flux-limiter f was artificially installed in order to avoid higher absorption rate and hydrodynamic efficiency.

$$q_L = f q_{FS}, \tag{6.11}$$

where f was evaluated to be 0.03–0.1 according to the difference of experiments. In hydrodynamic simulations, the following hear flus was modeled.

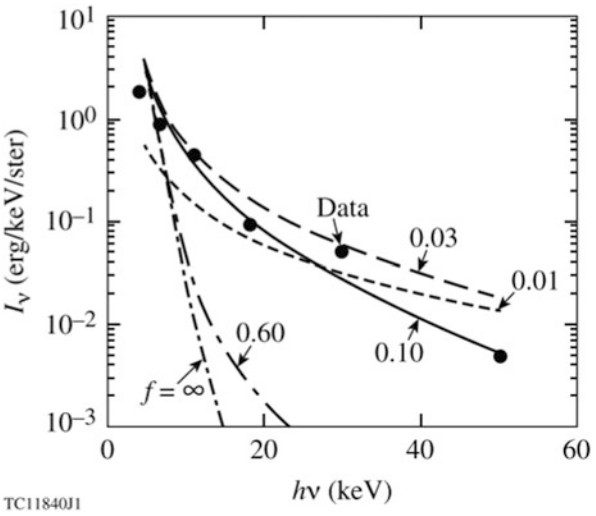

Fig. 6.1 Bremsstrahlung x-ray emission spectrum obtained in a laser produced plasma experiment (solid circles). The time integrated spectrum has been compared to hydrodynamic simulation results with different flux limiters. Spitzer-Harm diffusion model ($f = \infty$) is far from the experimental spectrum, while with smaller flux limiter the data can be explained computationally. Strong flux limitation was suggested in the early time from such comparison. Reprint with permission from Ref. [2]. Copyright 1998 by American Physical Society

$$q_{eff} = min(q_{FL}, q_{SH}) \tag{6.12}$$

or

$$q_{eff} = \frac{q_{SH} \cdot q_L}{q_{SH} + q_L}, \tag{6.13}$$

Then, the heat flow is small enough the **Spitzer-Harm diffusion** formula is used, but it is designed to limited by the limited flux.

In Fig. 6.1, calculated Bremsstrahlung emission spectrum I_ν versus photon energy $h\nu$ for different value of the flux limiter f is compared to the experimental data (solid circles). It is clear that simulation without the flux limiter results very low temperature in the Bremsstrahlung emission, while as the flux limiter increase hard x-ray emission reproduced as shown in Fig. 6.1. It is too early to conclude that in the experiment the flux is limited as $f = 0.01$–0.03. Such comparison of simulation to a variety of experimental results, however, had required to improve the mathematical model of the diffusion by electron heat conduction in high-intensity laser plasma interacting plasmas.

6.1.3 Mathematical Derivation of Spitzer-Harm Diffusion

In order to know the reason for the flux limit and the limiting condition of the validity of the diffusion approximation (6.10), let us repeat the mathematical process for deriving the diffusion model for the electron heat conduction.

Mathematical derivation of **Spitzer's heat flux** can be done by starting with the following kinetic equation of Vlasov equation with **Krook collision operator**.

$$\frac{\partial}{\partial t}f + \boldsymbol{v}\cdot\nabla f - \frac{e}{m}\boldsymbol{E}\cdot\frac{\partial}{\partial \boldsymbol{v}}f = -\nu_c(f - f_M) \tag{6.14}$$

where **E** is electrostatic field generated by charge separation due to electron motion by heat flux and f_M is local Maxwell distribution. The collision frequency ν_c is due to electron-ion and electron-electron collisions to be fixed so that they are derived by Fokker-Planck equation as a function of velocity as shown later.

In solving (6.14), space dependence is assumed one-dimensional in the x-direction and the velocity distribution function is assumed to consist of two terms; the isotropic component and the small anisotropic component.

$$f(x, v, \mu) = f_0(x, v) + \mu f_1(x, v) \tag{6.15}$$

$$\mu = cos\theta_v \tag{6.16}$$

where f_0 and f_1 are functions of only the absolute value of the velocity in **v**-space. The angle dependence of the velocity space is assumed only by θ_v, velocity angle along the x-direction as shown in Fig. 6.2. Inserting (6.15) to (6.14) yields

$$\begin{aligned}\frac{\partial}{\partial x}[v\mu(f_0 + \mu f_1)] - \frac{e}{m}E\frac{\partial}{\partial v}[\mu(f_0 + \mu f_1)] \\ + \frac{e}{m}E\frac{1-\mu^2}{v}f_1 = -\frac{v}{\lambda_c}(f_0 - f_M + \mu f_1)\end{aligned} \tag{6.17}$$

where $\lambda_c = v/\nu_c$ is an effective mean free path for electrons with the velocity v.

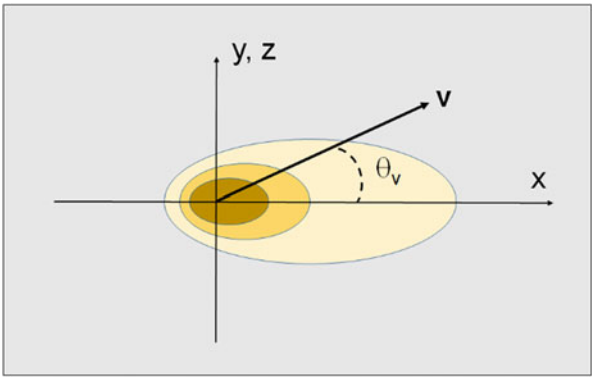

Fig. 6.2 Schematics of electron velocity distribution function to be modeled for Fokker-Planck equation, where non-uniformity of temperature is assumed to be in the x-direction and the velocity distribution is axially symmetric along the x-velocity axis. Space one-dimension and velocity space two-dimension are assumed

Taking the moment of velocity angle $\int_{-1}^{1} d\mu$ of (6.17), the first order distribution function is obtained as

$$\begin{aligned} f_1 &= -\lambda_c \left(\frac{\partial}{\partial x} - \frac{e}{m} \frac{E}{v} \frac{\partial}{\partial v} \right) f_M \\ &= -\frac{\lambda_c}{T_e} \left[eE + \frac{1}{2} \left(\frac{mv^2}{T_e} - 3 \right) \frac{\partial T_e}{\partial x} \right] f_M \end{aligned} \tag{6.18}$$

where f_0 is assumed to be a local Maxwellian f_M and the density is assumed to be uniform.

The electron current density is defined as

$$j_e = -e \int v_x f d^3\boldsymbol{v} = -\frac{4\pi e}{3} \int_0^\infty v^3 f_1 dv \tag{6.19}$$

Inserting (6.18) into (6.19), the current density is obtained in the form.

$$j_e = \sigma E - \beta \frac{dT_e}{dx} \tag{6.20}$$

where σ is the **electron conductivity** and β is the coefficient of **thermal current**. Note that the coefficients σ and β are functions of the temperature. Once there is a current flow in one-dimensional system, charge separation takes place. It is better to assume that this charge separation is induces the return current to keep the current neutral condition. Requiring the current neutral condition, the electric field is given in the form.

$$E = \frac{\beta}{\sigma} \frac{dT_e}{dx} \tag{6.21}$$

The electron heat flux is calculated as follows.

$$q_e = \frac{m}{2} \int v^2 v_x f d^3\boldsymbol{v} = \frac{4\pi m}{6} \int_0^\infty v^5 f_1 dv \tag{6.22}$$

Inserting (6.18) into (6.22) and eliminating E with (6.21), the heat flux (6.22) can be obtained in the form.

$$q_e = \gamma j_e - K_e \frac{dT_e}{dx} \tag{6.23}$$

where γ is a constant and K_e is the electron heat conduction coefficient. Requiring the current neutral condition, the electron heat flux is given in the form:

$$q_e = -K_e \nabla T_e \tag{6.24}$$

In the precise calculation including electron and ion contribution to the effective mean-free path in (6.18), the heat flux derived by Spitzer-Harm has the following form [3].

$$\boldsymbol{q}_{SH} = -\frac{128(Z+0.24)}{3\pi(Z+4.2)}\lambda_{SH} n_e v_e \nabla T_e \tag{6.25}$$

where λ_{SH} is the Spitzer-Harm mean free path,

$$\lambda_{SH} = \frac{3}{4\sqrt{2\pi}Z}\frac{1}{n_e b_0^2 ln\Lambda} \tag{6.26}$$

where the Coulomb impact radius defined in Chap. 2 in Volume 1 is given as b_0 satisfying the relation.

$$\frac{e^2}{4\pi\varepsilon_0 b_0} = m v_e^2 = T_e \tag{6.27}$$

In (6.25), the Z is the charge state for partially ionized plasma and the Z-dependence of the coefficient stems from the different ratio between the electron and ion contribution to Coulomb scattering. It is useful to express the form (6.25) as

$$q_{SH} = -a_0 \frac{\lambda_{SH}}{L_T} q_{FS} \tag{6.28}$$

where a_0 is the coefficient in (6.25) and q_{FS} is called **free-streaming flux** defined as

$$q_{FS} = n_e T_e v_e \tag{6.29}$$

This free-streaming energy flux is frequently used as normalization value for electron heat flux. This is almost the maximum flux by the half of Maxwell distribution. So, any model for heat flux cannot be larger than q_{FS}. This indicates that the mean-free-path should be much shorter than the temperature gradient scale L_T defined in (6.6).

It is useful to note that the maximum electron heat flux is in general much smaller than the free-streaming flux for example as seen in Fig. 6.1. This is because the strong heat flux induces the electrostatic field inhibiting the large heat flow goes to one direction. The charge separation is very important to reduce the heat flux compared to the free-streaming value. This is not the case for charge neutral particles like photons as will be explained later in this Chapter. In the case of photon emission, it is easily seen near the plasma boundary that almost all photons flow freely in one direction.

6.1.4 Breakdown of Diffusion Approximation

We have to be careful that Spitzer-Harm diffusion formula of the electron heat flux derived in (6.24) has been obtained in (6.18) with the assumption that

$$f_0 \gg |f_1| \tag{6.30}$$

Inserting (6.21) into (6.18) it is possible directly evaluate the condition (6.30) for f_0 being Maxwellian.

$$\frac{f_1}{f_M} = \frac{\lambda_c(v_e)}{L_T}\left(\frac{v}{v_e}\right)^4\left[\left(\frac{v}{\sqrt{2}v_e}\right)^2 - 4\right] \tag{6.31}$$

where L_T is the gradient scale defined in (6.6).

It is clear that the distribution function becomes negative for the case of $|f_1/f_0| > 1$. The velocity dependent heat flux $v^5 f_1$ in (6.22) is found to have its maximum at $v = 3.4v_e$. Since the heat flux is the integral of large power of the velocity, the maximum heat flux is mainly due to the electrons with the velocity more than the thermal velocity. The effective mean free path of such electrons is $(3.4)^4 \sim 10^2$ time longer than the SH mean free path in (6.26). Inserting $v = 3.4v_e$ to (6.31), it is found that the perturbation of the distribution become larger than the Maxwell distribution $|f_1/f_0| > 1$ at the value of the mean free path.

$$\frac{\lambda_c(v_e)}{L_T} \cong 4 \times 10^{-3} \tag{6.32}$$

This means that the SH heat conduction model cannot be applicable for the temerature gradient shorter than that in (6.32). This is usual case of laser produced plasma, where laser heating energy is carried by heated electrons from near the cut-off density to the solid density surface. It is essential to model the heat flux in another way.

6.2 Vlasov-Fokker-Planck Equation

6.2.1 Boltzmann Equation

Boltzmann equation is a kinetic equation of particles under collisional process. It is well known that in case of highly ionized plasma Coulomb collision between ions and electrons can be approximated by Fokker-Planck differential form. It is better, however, to start from Boltzmann equation to show what approximation are used to

derive Fokker-Planck equation to study the electron energy transport in laser produced plasma. See Appendix-C.

Boltzmann equation is non-linear integral-differential equation and time-consuming computation is required to solve numerically. **Boltzmann equation** for Coulomb collision system in plasma is formally given to be:

$$\frac{\partial f}{\partial t} + \boldsymbol{v} \cdot \frac{\partial f}{\partial \boldsymbol{r}} - \frac{e}{m}\boldsymbol{E} \cdot \frac{\partial}{\partial \boldsymbol{v}} f = \left(\frac{df}{dt}\right)_{coll} = \left.\frac{df}{dt}\right|_{ei} + \left.\frac{df}{dt}\right|_{ee} \tag{6.33}$$

In RHS in (6.33), the collision terms of electrons with ions and with electrons are shown in the first and second terms, respectively.

Derive the collision term with assumption that only binary collision is enough to derive the collision term. Then, assume that binary collision changes the velocities of two particles before and after the collision. Consider the collision term of the electron distribution function with velocity **v** changes its velocity to **v**' by the collision of electron or ion with velocity $\mathbf{v}_s$ changing it to $\mathbf{v}_s$' after the collision. In what follows the subscribe "s" represents the both cases of collision with ion and electron.

$$\{\boldsymbol{v}, \boldsymbol{v}_s\} \rightarrow \{\boldsymbol{v}', \boldsymbol{v}_s'\} \tag{6.34}$$

The differential cross section of such binary collision $\sigma_s(\boldsymbol{\Omega})$ is given as the function of the relative orientation of the vectors $\mathbf{v}$-$\mathbf{v}_s$ and $\mathbf{v}'$-$\mathbf{v}_s'$, the unit vector of which is defined as $\boldsymbol{\Omega}$. Of course, the functional form, σ_s depends on the collision opponent is an electron or an ion. Then, it is easy to understand that the collision term is given in the form.

$$\left(\frac{df}{dt}\right)_{coll} = \sum\nolimits_{s=i,e} \int d\boldsymbol{\Omega} \int d\boldsymbol{v}_s \sigma_s(\boldsymbol{\Omega}) |\boldsymbol{v} - \boldsymbol{v}_s| \left(f' f_s' - f f_s\right) \tag{6.35}$$

In (6.35),

$$\begin{aligned} f &\equiv f(\boldsymbol{r}, \boldsymbol{v}, t), \quad f' \equiv f(\boldsymbol{r}, \boldsymbol{v}', t) \\ f_s &\equiv f_s(\boldsymbol{r}, \boldsymbol{v}_s, t), \quad f_s' \equiv f_s(\boldsymbol{r}, \boldsymbol{v}_s', t) \end{aligned} \tag{6.36}$$

The collision term (6.33) gives the change of the distribution function f after the collision with another or same particle with distribution f_s at the point **r** and time t. The term $f' f_s$' represents the gain to **v** from **v**' due to the collision with $\mathbf{v}_s$'. On the other hand, the term $f f_s$ represents the loss from **v** from **v**, after the collision with a particle with the velocity $\mathbf{v}_s$. Integrating by $\mathbf{v}_s$ provides all contribution from the particle in plasma at (**r**,t) position by the other electrons and ions. Since the integrand should be the collision frequency, it is proportional to $\sigma_s(\boldsymbol{\Omega})|\boldsymbol{v} - \boldsymbol{v}_s|$. The scattering cross section is given by Rutherford scattering formula.

6.2.2 Taylor Expansion of Collision Term

In the Coulomb scattering, the velocity change |Δ**v**| by one binary collision is sufficiently smaller than the velocity |**v**|. In such case, Boltzmann equation of (6.33) can be expanded with the small velocity change. When the probability density of the small change of Δ**v** due to the scattering of the distribution of **v** is W(**v**, Δ**v**), the following relation holds

$$f(\boldsymbol{v},\boldsymbol{r},t+\Delta t)=\int f(\boldsymbol{v}-\Delta\boldsymbol{v},\boldsymbol{r},t)W(\boldsymbol{v}-\Delta\boldsymbol{v},\Delta\boldsymbol{v})d(\Delta\boldsymbol{v}) \tag{6.37}$$

It is important to note the physical difference of (6.1) and (6.33). In case of random walk in real space (6.1), the mean random step <Δx> can be easily break the condition for approximation (6.6) and the breakdown of the diffusion approximation appears as in Spitzer-Harm model. However, the random scattering in the velocity space is always valid as long as Coulomb scattering is considered. So, it is expected that Taylor expansion of (6.37) is applicable even to the case with steep temperature gradients. This is because the velocity change in most of Coulomb scattering is due to small angle scattering.

In what follows, only the change of distribution function of electrons by the small angle scattering is formulated for simplicity. Assuming small angle scattering and considering that the distribution function change with short time interval Δt, (6.37) reduces to the Taylor expansion form to Δt and Δ**v** in the form.

$$\begin{aligned} f(\boldsymbol{v},\boldsymbol{r},t+\Delta t) \;=\; & \int f(\boldsymbol{v},\boldsymbol{r},t)W(\boldsymbol{v},\Delta\boldsymbol{v})-\Delta\boldsymbol{v}\cdot\frac{\partial}{\partial\boldsymbol{v}}\left[f(\boldsymbol{v},\boldsymbol{r},t)W(\boldsymbol{v},\Delta\boldsymbol{v})\right] \\ & +\frac{1}{2}\sum_i\sum_k\Delta v_i\Delta v_k\frac{\partial^2}{\partial v_i\partial v_k}\left[f(\boldsymbol{v},\boldsymbol{r},t)W(\boldsymbol{v},\Delta\boldsymbol{v})\right]\; d(\Delta\boldsymbol{v}) \end{aligned} \tag{6.38}$$

From (6.38) the collision term in a differential form to Coulomb interacting system is obtained.

$$\left(\frac{df}{dt}\right)_{coll}=\frac{\partial}{\partial v_i}\left[\left\langle\frac{\Delta v_i}{\Delta t}\right\rangle f(\boldsymbol{v},\boldsymbol{r},t)\right]+\frac{1}{2}\sum\nolimits_i\sum\nolimits_k\frac{\partial^2}{\partial v_i\partial v_k}\left[\left\langle\frac{\Delta v_i\Delta v_k}{\Delta t}\right\rangle f(\boldsymbol{v},\boldsymbol{r},t)\right] \tag{6.39}$$

where $<\ >$ represents the ensemble average of the terms. In case of one-dimension in the real space, the velocity space can be approximated axial symmetric with the axis of the inhomogeneous direction as shown in Fig. 6.2. The velocity space is two-dimensional in the cylindrical coordinate system (v_r, θ_v). The characteristics of Fokker-Planck equation are as follows:

1. The distribution function never becomes negative,
2. The equation satisfies the conservation of particle, momentum, and energy locally.
3. It satisfies Boltzmann's H-theorem. Even starting from any distribution function, the final distribution function becomes Maxwellian in LTE condition.

6.2.3 Derivation of Fokker-Planck (FP) Equation

What Fokker-Planck (FP) equation says is that any random force in Brownian motion reduces to the combination of the friction term and diffusion term.

After a long algebra shown in [4, 5], FP equation is found to have the following form.

$$\left(\frac{\partial}{\partial t}f\right)_{coll} = -\Gamma\frac{\partial}{\partial v_k}\left(\frac{\partial H}{\partial v_k}f\right) + \frac{1}{2}\Gamma\frac{\partial^2}{\partial v_k \partial v_j}\left(\frac{\partial^2 G}{\partial v_k \partial v_j}f\right) \tag{6.40}$$

where G is derived from Rutherford scattering cross section and H and G are given as

$$\Gamma = \frac{Z^2 e^4}{4\pi\varepsilon_0^2 m^2}\,ln\Lambda \tag{6.41}$$

$$H(\boldsymbol{v}) = Z_s^2\left(\frac{m+m_s}{m_s}\right)\int\frac{f_s(\boldsymbol{v}_s)}{|\boldsymbol{v}-\boldsymbol{v}_s|}d\boldsymbol{v}_s \tag{6.42}$$

$$G(\boldsymbol{v}) = Z_s^2\int f_s(\boldsymbol{v}_s)|\boldsymbol{v}-\boldsymbol{v}_s|d\boldsymbol{v}_s \tag{6.43}$$

It is noted that the definition H and G are called the **Rosenbluth potentials** [6].

It is known that the first term of RHS in (6.40) is the dynamical friction and the second one is the diffusion term in the velocity space. The Fokker-Planck equation assumes only the scattering by the binary Coulomb collision, therefore, in the system of two kind of particles like fully-ionized ions and electrons, we have to solve the equation for electron distribution function changing in time by scattering due to electron-electron (e-e), electron-ion (e-i). It is noted that in the case of e-e scattering, (6.40) is a nonlinear equation to the distribution function.

6.2.4 Linearized FP Model

It is time consuming to solve exactly (6.40) at each time step in FP computer simulation. It is better to consider some approximation to make numerical method

much easier in solving (6.40). For the present problem of electron heat transport, the following two assumptions can be adopted.

1. In the collision with the ions, it is assumed that $m_i >> m_e$ and energy transfer between electron and ions is neglected. This means the ions are regarded to be particles at rest. Then, the ion collision contributes to only the momentum change and no energy change of scattered electrons.
2. The nonlinear term in calculation of H and G in (6.42) and (6.43) are assumed by replacing f_s is local Maxwell distribution. In addition, $|\boldsymbol{v} - \boldsymbol{v}_s|$is replaced with $\mathbf{v}$ in the both definitions. This is valid because the electron heat transport is sensitive to the collision of large v component by the electron with lower energy.

The 1st and 2nd derivatives in velocity space (6.40) can be separated to the changes in the absolute value of v (energy) and the scattering to perpendicular direction without changing energy. The former is only due to electron-electron scattering and the latter is due to both. It is possible to separate them into two parts as shown below.

The scattering term can be given as

$$\left.\frac{df}{dt}\right|_{ei,ee} = \sum\nolimits_{s=i,e} \frac{\partial}{\partial v_\perp}\left(D_s \frac{\partial}{\partial v_\perp} f\right) \tag{6.44}$$

$$\left.\frac{df}{dt}\right|_{ee} = \frac{\partial}{\partial v_\parallel}\left(F_e f + D_e \frac{\partial}{\partial v_\parallel} f\right) \tag{6.45}$$

In what follows, the distribution function is assume to be cylindrically symmetric in the velocity space along the x-direction, where the plasma parameters change in space locally in the x-direction.

By use of Taylor expansion with care of the fact that hear flux is due to high velocity component, while the collisions are mainly with electrons with relatively low velocity, the following approximated linear form of Fokker-Planck equation is obtained

$$\begin{aligned} &\frac{\partial}{\partial t} f + v\mu \frac{\partial}{\partial x} f - \frac{e}{m} E\left(\mu \frac{\partial}{\partial v} + \frac{1-\mu^2}{v} \frac{\partial}{\partial \mu}\right) f \\ &= \frac{v}{2\lambda_S(v)} \left\{ \frac{\partial}{\partial \mu}\left(1-\mu^2\right) \frac{\partial}{\partial \mu} f \right\} + \frac{v^2}{\lambda_f(v)} \left(\frac{\partial}{\partial v} \frac{{v_e}^2}{v} \frac{\partial}{\partial v} + \frac{\partial}{\partial v} \right) f \end{aligned} \tag{6.46}$$

The angle of the velocity space is replaced with a definition

$$\mu = \cos\theta \tag{6.47}$$

It is noted that the following formula was used in (6.46).

$$\frac{\partial}{\partial v_x} = \mu \frac{\partial}{\partial v} + \left(1-\mu^2\right) v^{-1} \frac{\partial}{\partial \mu} \tag{6.48}$$

In the RHS of (6.46), the first term is the effective mean free path by scattering.

$$\lambda_S(v) = \frac{m^2 v^4}{4\pi n_e (Z+1) e^4 \, ln\Lambda} \tag{6.49}$$

This is due to the scattering of electrons by ions and background electrons. The second term is due to the frictional force among electrons.

$$\lambda_f(v) = \frac{m^2 v^4}{4\pi n_e e^4 \, ln\Lambda} \left[= (Z+1)\lambda_S(v) \right] \tag{6.50}$$

It is mathematically clear that the 1st term in RHS of (6.46) is diffusion in angular space without energy change, while the 2nd term is the change in v-space with change of energy. It is noted that the RHS of (6.46) disappears when the electron distribution function is a Maxwellian distribution with thermal velocity v_e. The second term in (6.46) is derived by assuming that the counter electrons are in local Maxwellian.

In order to check the validity of several heat conduction models, it has been done to solve directly the FP equation numerically as reference case. The property that the Legendre functions is the eigen function of 1st term of RHS of (6.46) has been well used. The distribution function is expanded by **Legendre polynomial** as follows:

$$f = \sum\nolimits_{n=0}^{N} f_n(x, v, t) P_n(\mu) \tag{6.51}$$

Inserting (6.51) into (6.46) and using the following mathematical formula to Legendre function.

$$\begin{aligned} \mu P_n &= \frac{1}{2n+1}\left[(n+1)P_{n+1} + nP_{n+1}\right] \\ \left(\mu^2 - 1\right)\frac{\partial}{\partial \mu} P_n &= n(\mu P_n - P_{n-1}) \\ \frac{\partial}{\partial \mu}\left\{\left(1-\mu^2\right)\frac{\partial}{\partial \mu} P_n\right\} &= -n(n+1)P_n \end{aligned} \tag{6.52}$$

It is possible to make (6.46) as functions only proportional to Legendre function regarding the terms including μ. Comparing the term proportional to the same order of Legendre functions, the following coupled equations are obtained.

$$\frac{\partial}{\partial t}f_n + v\frac{\partial}{\partial x}\left(\frac{n}{2n-1}f_{n-1} + \frac{n+1}{2n+3}f_{n+1}\right) - \frac{e}{m}E\left[\frac{n}{n-1}\left(\frac{\partial f_{n-1}}{\partial v} - \frac{n-1}{v}f_{n-1}\right) + \frac{n+1}{2n+3}\left(\frac{\partial f_{n-1}}{\partial v} + (n+2)\frac{f_{n+1}}{v}\right)\right] = -\frac{v}{2\lambda_S(v)}n(n+1)f_n + \frac{v^2}{\lambda_f(v)}\left(\frac{\partial}{\partial v}\frac{v_e{}^2}{v}\frac{\partial}{\partial v} + \frac{\partial}{\partial v}\right)f_n \tag{6.53}$$

This can be numerically solved by coupling with Poisson equation.

$$\varepsilon_0\frac{dE}{dx} = 4\pi e n_e\left(\int f d^3\boldsymbol{v} - 1\right) \tag{6.54}$$

FP equation shown in (6.53) looks like linear coupled equations for f_n ($n = 0 \sim n_{max}$), where n_{max} is the maximum number of n to be solved. However, the electrostatic field generated by the electron heat flux is given by the sum of all Legendre component f_n, consequently for example some iterative process is required to obtain at each time step consistently. In addition, very fast oscillation by plasma waves is also generated by charge separation. In order to weaken such oscillation effect, some idea is required in numerically solving (6.53) and (6.54).

FP Eq. (6.53) has been solved numerically with numerically reducing the plasma oscillation frequency [7]. The plasma is initially uniform in density and temperature. The temperature in the region around the one boundary is quickly heated to 4 times, and the time progress of heat flux and temperature have been calculated. The Legendre components up to n = 8 have been solved in (6.53). In addition, Poisson equation is solved with an artificial fraction r = .0011 as a factor in RHS in (6.54). Plots of temperature $<v^2>$ and heat flux $<v^2 v_x>$ as function s of space x at three different times are shown in Fig. 6.3. It is seen that the heat flux is maximum near the heated region and the heat flux propagates from the left to the right in time.

In Fig. 6.4, the calculated heat flux is plotted at two typical time with symbols (x) and (o) as functions of the local temperature gradient length L (=L_T) normalized by the local mean free path λ. The hear flux Q by FP calculation is normalized by the local free streaming flux $Q_f = q_{FS}$ defined by (6.8) in the vertical axis. In Fig. 6.4, the solid line is the relation of heat flux by SH model (6.24). It is found that the heat flux is saturated around 0.1 q_{FL} for $\lambda/L_T < 0.01$ in the FP calculation. In the next paper by Bell, he has carried out FP simulation for the density and temperature profile more realistic to the laser ablation plasma. He found the flux limitation of about f = 0.03 for $\lambda/L_T < 0.01$ [8].

It is noted that the flux limit factor in Fig. 6.1 seems to be f = 0.02–0.01 for the best fit to the experiment, but the flux limiter is an ad hoc parameter and a different limiter may happen depending on the plasma parameters. These fact means SH diffusion model is not acceptable even in a simple model for the sharp temperature gradient satisfying $\lambda/L_T < 0.01$, and it is required to derive another heat flux model easily installable into hydrodynamic simulation code. This will be discussed soon.

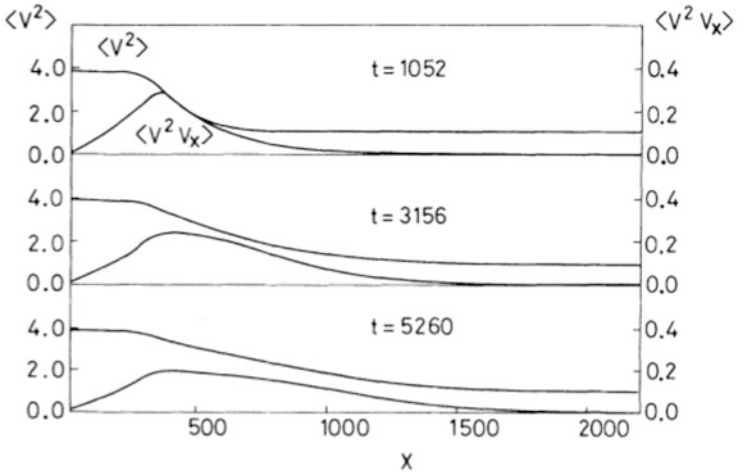

Fig. 6.3 Time evolution of an effective temperature $\langle v^2 \rangle$ and heat flux $\langle v^2 v_x \rangle$ obtained by a model simulation for Fokker-Planck equation of electron in constant density. At the left boundary, the effective temperature is kept four times of that at the right boundary. The heat wave propagates from the left to right. Reprint with permission from Ref. [7]. Copyright 1998 by American Physical Society

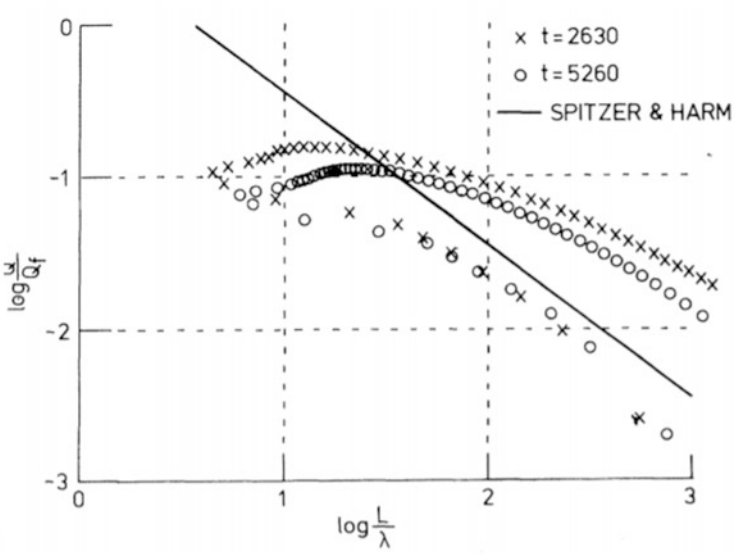

Fig. 6.4 The heat flux of Fokker-Planck simulation normalized with the free streaming flux is plotted at two different times as a function of measured temperature gradient length divided by the local electron mean-free-path. The solid line is the relation of Spitzer-Harm (SH) diffusion. The simulation data are higher than SH flux near the front of the heat flux, while it is automatically limited around f=0.1 to change to the reduced flux in the higher temperature region. This indicate that the local assumption of heat flux defined with the first derivative to space x is not valid. Reprint with permission from Ref. [7]. Copyright 1998 by American Physical Society

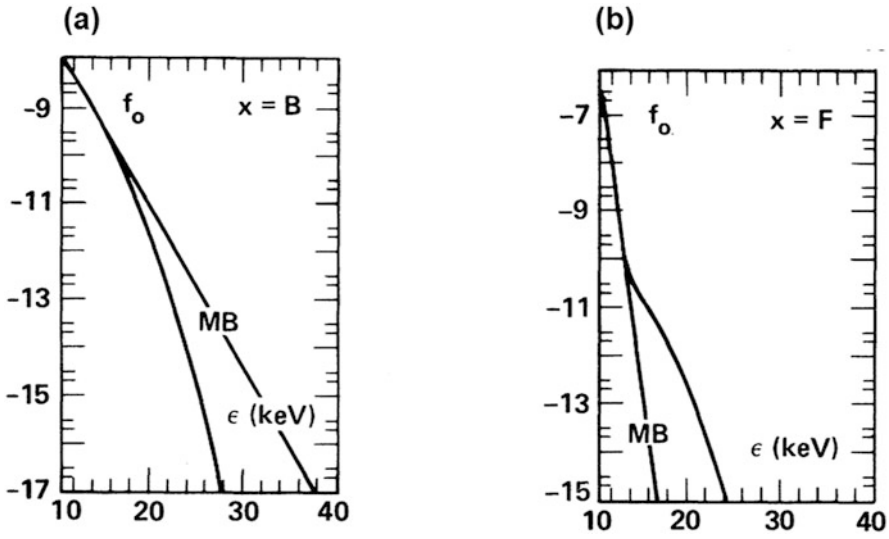

Fig. 6.5 The double functions in Fig. 6.4 stems from the non-Maxwell distribution of f_0(v). The distribution functions obtained by solving FP equation in more relativistic density and temperature profiles are shown. (**a**) and (**b**) are the distribution functions at the laser heated low density region and the heat wave front in the high-density region, near the ablation front, respectively. Reprint with permission from Ref. [9]. Copyright 1998 by American Physical Society

Not only the limitation of the electron heat flux, but also the hysteresis of the heat flux is also seen in Fig. 6.4. Especially, the heat flux is enhanced than SH flux at the heat front region, right region in Fig. 6.3. Enhanced heat flux is due to the high-energy component coming into the cold region from the hotter region, because the mean free path with velocity v is proportional to v^4 and high-energy components freely penetrate in the front region. Such component contributes the preheating of cold region. It is very important if the absorbed laser energy is carried by heat flux, while the high-density and cold region has to be controlled to as cold as possible.

The hysteresis property stems from the non-Maxwell distribution of f_0(v). The distribution functions obtained by solving FP equation in more relativistic density and temperature profiles are shown in Fig. 6.5 [9]. Figures (a) and (b) are the distribution functions at the laser heated low density region and the heat wave front in the high-density region, near the ablation front, respectively. The distribution function near the heating region has less high-energy component than the local Maxwell distribution, therefore the heat flux is reduced than SH model. On the other hand, near the heat front with enhanced high-energy component is produced by electrons coming from the heated region without enough scattering. This enhances the heat flux than SH model in the cold region. This is called **preheating**.

Since FP simulation is time consuming calculation and is not realistic to couple it with hydrodynamic codes. There have been proposed better modeling reproducing almost FP result with simple mathematical models. In what follows, such better models to provide the typical properties of the flux limitation and preheating are reviewed. As summary, the following two characters should be noted.

1. Heat flux is limited in laser, hearting region because of the violation of SH model (flux limitation)
2. Heat flux is higher than SH flux near the heat front region (nonlocal transport)

6.2.5 *Flux Limit Properties*

Before going to the advanced models for the electron heat flux in laser produced plasma, consider the difference of the heat fluxes mentioned so far from the FP simulation result. The reduction of heat conductivity in FP simulation has been studied by assuming sinusoidal temperature perturbation [10]. In this case, the heat diffusion with SH heat flux is solved numerically to compare to FP simulation result.

$$\frac{3}{2}n\frac{\partial T}{\partial t} = -\frac{\partial}{\partial x}q_{SH}, \quad q_{SH} = -\kappa_{SH}\frac{\partial}{\partial x}T \tag{6.55}$$

The initial condition is

$$T(0,x) = T_0 + \delta T(0)\, exp(ikx) \tag{6.56}$$

From the time progress of heat conduction, it is clear that the relation

$$\delta T(t) \propto exp(-\gamma t) \tag{6.57}$$

is observed. The decay rate is directly related to the heat conduction coefficients for SH model and can be derived for FP simulation as follows.

$$\gamma_{SH} = 2k^2\kappa_{SH}/3n, \quad \gamma_{FP} = 2k^2\kappa_{FP}/3n \tag{6.58}$$

Then, it is possible to define the following normalized value for measuring the flux reduction in FP simulation.

$$\frac{\kappa_{FP}}{\kappa_{SH}} \tag{6.59}$$

The simulation result is plotted with solid circles in Fig. 6.6 [10]. In Fig. 6.6, the solid curve is a fitting curve and the relation is

$$\frac{\kappa_{FP}}{\kappa_{SH}} = \frac{1}{1 + (30k\lambda_e)^{4/3}} \tag{6.60}$$

Further study showed that the FP simulation result can also fit with the following simpler formula [3].

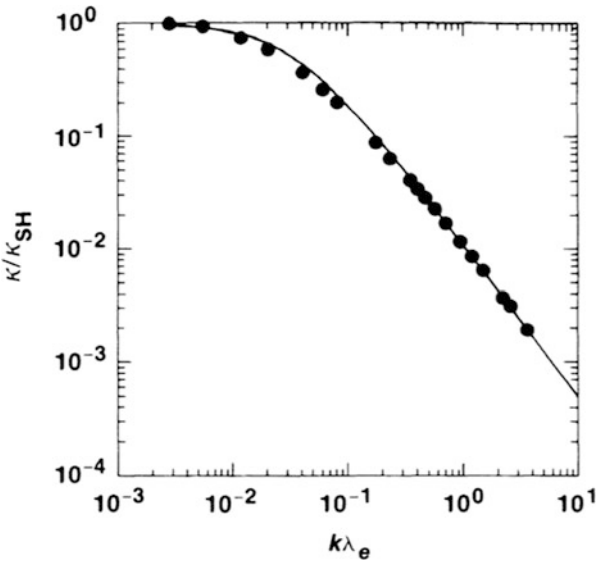

Fig. 6.6 Wavenumber dependence of an effective thermal conductivity obtained with Fokker-Planck (FP) simulation normalized by the thermal conductivity used in SH heat diffusion model. FP simulation has been done to the sinusoidal temperature variation as initial condition characterized with the wavenumber k. It is clearly seen that the flux is limited for steeper temperature gradient case. Reprint with permission from Ref. [10]. Copyright 1998 by American Physical Society

$$\frac{\kappa_{FP}}{\kappa_{SH}} = \frac{1}{1 + 60k\lambda_e} \tag{6.61}$$

For long wavelength perturbation, the heat conductivity is well modeled with SH model, but the conductivity is strongly reduced at short wavelength perturbation. It is informative to compare this relation (6.61) to the case of flux limited heat flux easily calculated to be

$$\frac{\kappa_{FL}}{\kappa_{SH}} = \frac{1}{1 + f^{-1}k\lambda_e} \tag{6.62}$$

It should be noted that the flux limiter $f = 1/60$ (=0.017) well reproduces the FP result. This value of f is consistent to the comparison with the experiment shown in Fig. 6.1.

6.3 Flux-Limit and Nonlocal Models

6.3.1 LMV Nonlocal Model

In an early time, Luciani, Mora, and Virmont (LMV) proposed the following model expression for nonlocal transport [11]. Stationary state is assumed for the heat flux.

$$q_e(x) = \int_{-\infty}^{\infty} q_e(x + \Delta x) W(\Delta x, x) d(\Delta x) \tag{6.63}$$

The **LMV nonlocal heat flux** is given in the form after replacing the variable x' = x + Δx and approximating the heat flux in the integral with SH formula (6.10).

$$q_{LMV}(x) = \int_{-\infty}^{\infty} q_{SH}(x')W(x',x)d(x') \tag{6.64}$$

where the **propagator** (**kernel**) of the heat flux is defined [11].

$$W(x,x') = \frac{1}{2\lambda(x')}\, exp\left(-\left|\int_{x'}^{x} \frac{n_e(x'')}{n_e(x')}\,\frac{dx''}{\lambda(x')}\right|\right) \tag{6.65}$$

The effective mean free path in the propagator is defined as

$$\lambda = a(\lambda_s\lambda_f)^{1/2}\Big|_{v=v_e}, \quad a = 32 \tag{6.66}$$

where λ_s and λ_f are velocity-averaged mean free paths calculated by scattering and friction given in (6.49) and (6.50), respectively. The coefficient "a" in (6.66) is the adjustable parameter and derived by comparison with FP simulations.

6.3.2 *Probability Density of Diffusion*

In order to investigate the physical property of the propagator of the heat flux model in (6.64), let us Fourier transform of the LMV heat flux q_{LMV} in a uniform density and constant mean-free-path.

$$q_{LMV}(x) = \int_{-\infty}^{\infty} W(\Delta x)q_{SH}(x+\Delta x)d(\Delta x) \tag{6.67}$$

where we assume for simplicity,

$$W(\Delta x) = \frac{1}{2\lambda}\, exp\left(-\frac{\Delta x}{\lambda}\right) \tag{6.68}$$

Fourier transformation of the propagator is defined as

$$\Psi(k) = \int_{-\infty}^{\infty} W(x)e^{-ikx}dx \tag{6.69}$$

Carrying out the Fourier transformation of (6.1), we can use of the **convolution integral** in Fourier transformation.

$$G(k)H(k) = \frac{1}{\sqrt{2\pi}} \int_{-\infty}^{\infty} \left[\int_{-\infty}^{\infty} g(x-y)h(y)dy \right] e^{-ikx} dx \tag{6.70}$$

By use of the convolution relation, (6.67) can be easily transformed to Fourier relation.

$$Q_{LMV}(k) = \Psi(k) Q_{SH}(k) \tag{6.71}$$

where the Fourier function is defined as

$$Q_{LMV}(k) = \int_{-\infty}^{\infty} q_{LMV}(x) e^{-ikx} dx \tag{6.72}$$

The Fourier function of the propagator is the same as the heat conductivity ratio and the case of LMV model can be obtained as

$$\frac{\kappa_{LMV}}{\kappa_{SH}} \equiv \Psi(k) = \frac{1}{1 + (k\lambda)^2} \tag{6.73}$$

where the following relation has been used.

$$\Psi(k) = \frac{1}{2\lambda} \int_{-\infty}^{\infty} e^{-|x|/\lambda - ikx} dx = \frac{1}{2} \left(\frac{1}{1 + ik\lambda} - \frac{1}{-1 + ik\lambda} \right) \tag{6.74}$$

Although the physical meaning of the LMV model is easily understand and reasonable to be used. However, the flux limit spectrum (means k-dependence) is different from FP calculation shown in (6.61). This is speculated that even with LMV model, the big difference of the mean-free-path on the velocity is not modeled. It suggests that it is better to develop the model for multi-group electron transport, where the heat flux is defined for each velocity component.

In Fig. 6.7 [3], the normalized Fourier functions of the heat conductivity are compared for LMV model and FP result. The LMV model reduces faster than FP result for l/L_T gets to large, too much heat flux is obtained. The other curve AWBS model is from [12] which has improved the LMV model, consequently better modeling.

We have investigated how to improve SH heat conduction model to allow the flux limitation as suggested in experiment and FP simulation. However, even if the flux limitation is reproduced, the electron kinetic effect is also very important to provide the preheating effect. This should be also modeled in an appropriate conduction formula. For this purpose, we need a model allowing the difference of mean free path for difference of velocity of electrons. Let us see more modernized model for heat conduction by electrons.

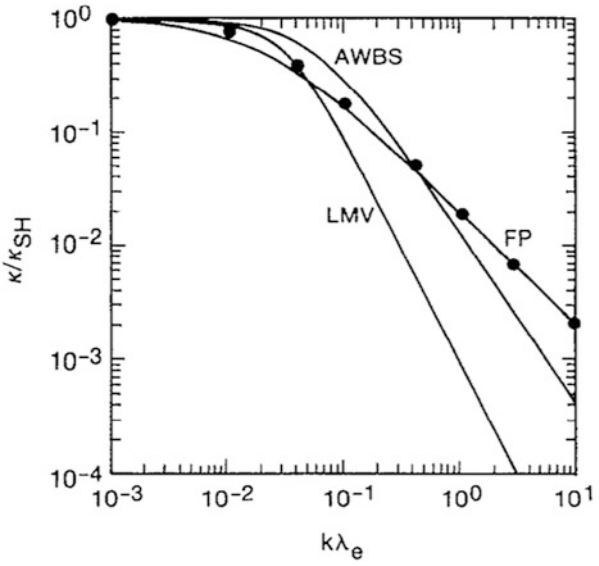

Fig. 6.7 Two different non-local heat flux models are compared to FP simulation result shown in Fig. 6.6. The integration form of heat flux LMV in (6.64) also reproduces the flux limitation property, while a difference is seen in the figure. AWBS model looks well reproduce FP simulation result. Reprint with permission from Ref. [11]. Copyright 1998 by American Physical Society

6.4 Comparison with an Experiment

The nonlocal transport model and Fokker-Planck calculations have been compared to measured temperature profiles of electron temperature in laser heated nitrogen gas jet plasma [13]. Gas jet is irradiated with 1ω laser and the heat wave region are irradiated with a short pulse 2ω laser at the same time to measure Thomson scattering and Rayleigh scattering spectra of 2ω lights. The probe beam moves to cover the space of about 2 mm in front of the laser heating plasma region. Simply saying, the principle of Thomson scattering is as follows. The probe beam is scattered by the ion acoustic waves in the plasma and the probe beam is scattered with frequency shift which is the function of the dispersion relation of the ion acoustic wave. Since the ion acoustic wave has its phase velocity proportional to the square root of the electron temperature, the spatial profile of the electron temperature is inferred from the spatial profile of the phase shift [13].

In Fig. 6.8, the experimental data of electron temperature is compared for $t = 0.3$ ns and 1.5 ns. The heating laser has a Gaussian shape with 1.4 ns half width and intensity of 1.5×10^{14}W/cm^2. So, $t = 0.3$ ns is at the beginning and $t = 1.5$ ns is almost at the peak intensity. The typical electron density measured by Rayleigh scattering is 10^{19} cm^{-3}. When the laser intensity is week as $t = 0.3$ ns, the experimental data with error bars are well reproduced with LASNEX and it is almost independent of the flux limiter. At $t = 1.5$ ns, on the other hand, the experimental data differ substantially from LASNEX results with the flux limiter 0.05 and 1.0. Fokker-Planck simulation of 2D SPARK is used to compared to obtain a good agreement with the experimental data. This suggest that LASNEX code does not provide the heat flux penetrating to the deeper region and the flux limit $f = 0.05$ too much prevents the heat loss from the heating region.

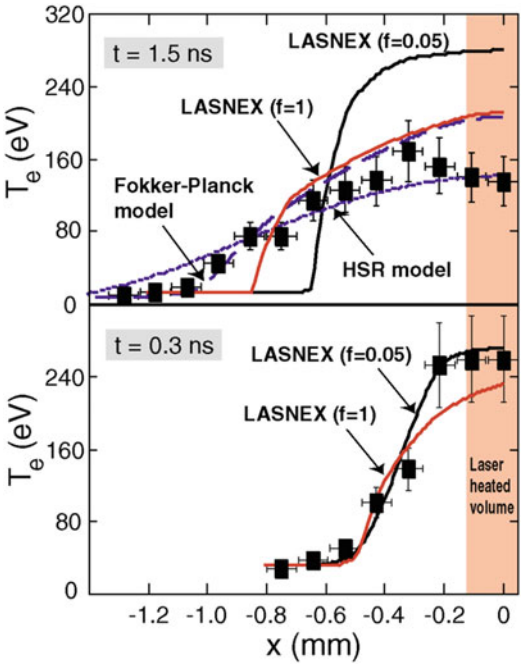

Fig. 6.8 Experimental data of electron temperature profiles at two different times (0.3 ns and 1.5 ns). The data are shown with solid squares with error bars. The temperature profile near the peak of laser pulse (t = 1.5ns) is compared to the flux limited diffusion model with f = 1 and 0.05 shown with red and black lines, respectively. The Fokker-Planck simulation result is plotted with the dashed black line. HSR model can also reproduced the data well. Reprint with permission from Ref. [14]. Copyright 1998 by American Physical Society

In order to validate a nonlocal model discussed previously with such comparison, the same type of form (6.64) has been calculated. It is called "hot spot relaxation (HSR)" model [14]. In HSR, the kernel W(x', x) is modified from (6.65) so that Fourier spectrum of K/K_{SH} is designed to be

$$\frac{K}{K_{SH}} = \frac{1}{1 + (ak\lambda_e)^{0.9}}, \qquad \lambda_e = \sqrt{Z}\lambda_{ei}, \qquad k\lambda_{ei} \le 1 \tag{6.75}$$

where a = 10(Z + 5)/(Z + 12). HSR roughly reproduce Fourier spectrum of FP simulation result shown in Fig. 6.6.

6.5 Multi-group (SNB) Model

The kernel (6.68) is physically well understood and it may give a good model for a single electron group. As we see, it can give the flux-limit property, although slightly different from FP numerical result. It is reasonable to extend it to the case of multi-group electrons, where electron velocity distribution is divided to N group and the propagator is defined as function of the velocity. Then, the preheating by long mean-free-path electrons can be included in the model as well as the flux-limiting property. There have been proposed several methods for such modeling, however, the

difference is mathematical method. Therefore, the idea on how to extend it to the multi-group case is explained for so-called **SNB model** by Schurtz, Nicolai, and Busquet [15].

Before explaining the derivation of SNB model, it is useful to see the comparison of SNB model to FP and SH results. In Ref. [16], the models are compared to the situation relating to the laser plasma. In Fig. 6.9, "Heat bath problem" is shown at $t = 80$ ps after starting with the red curve of the temperature. The black is FP and blue is SNB result. It is well seen that the preheating is well given as that by FP calculation. The heat flux at this point at 10 ps is plotted in Fig. 6.10. The black is SH, red is FP and blue is SNB models, respectively. This result explains the flux limit and preheating well. The peak flux is limited compared to the SH model and the pre-heating in the region for $x > 500$ μm is reasonably predicted by SNB model.

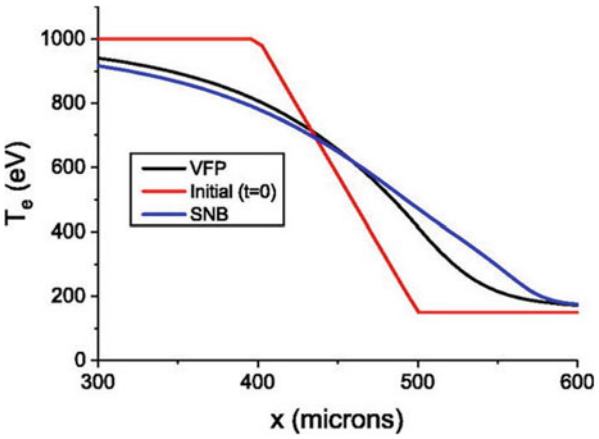

Fig. 6.9 Model simulation of VFP and SNB model starting from the initial temperature distribution plotted with red line. It is shown that SNB model reproduces well the VFP simulation. Reprint with permission from Ref. [17]. Copyright 1998 by American Institute of Physics

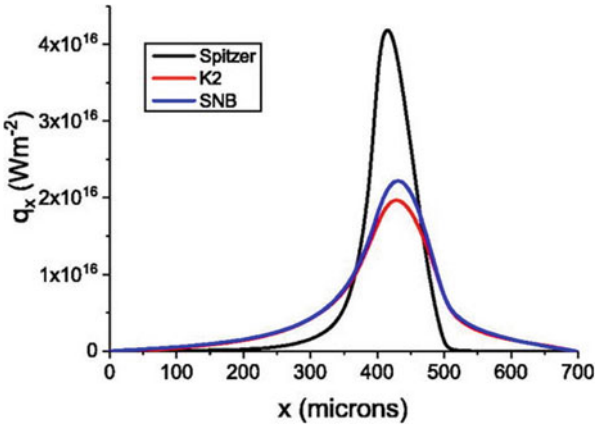

Fig. 6.10 Heat flux distribution at the same time as in Fig. 6.9. The red line is from K2 code of VFP simulation and the blue line is SNB, which reproduces well the VFP result. The black line is from SH heat diffusion model. It is clear that SH overestimates the heat flux and does not show the preheating compared to VFP, while SNB well reproduces these two effects. Reprint with permission from Ref. [17]. Copyright 1998 by American Institute of Physics

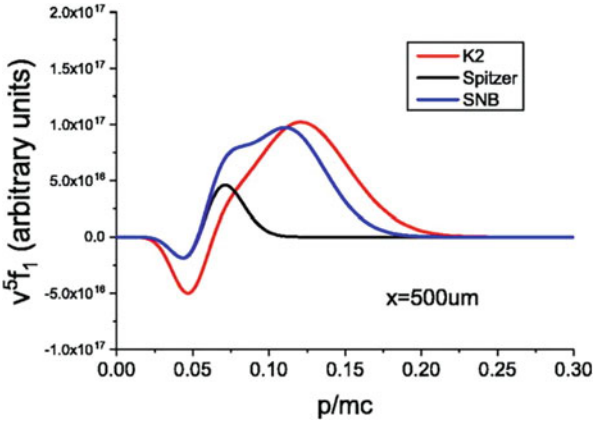

Fig. 6.11 The velocity dependence of $v^5 f_1$ at the point of x=500mm at the time of previous two figures. Near this point the preheating by higher velocity electrons becomes important in K2 (VFP) simulation and SNB model can well reproduce such preheating as shown with the blue line. Reprint with permission from Ref. [17]. Copyright 1998 by American Institute of Physics

The velocity dependence of heat flux is compared in Fig. 6.11 for SH (black), FP (red), and SNB (blue) models at the heat front x = 500 μm at 10 ps. The f_1 of SH is calculated with (6.31) and the sign change around v = 0.05c, and this is less evaluation of the preheating by high-energy electrons from the high-temperature region. FP shows enhanced component of heat flux by higher energy electrons, and this is well reproduced by SNB model.

In SNB model, the electron heat flux is given as the sum of all velocity groups, consequently the property of long mean free path of high energy electrons are well reproduced. Let us consider the physics of SNB model. Note that SNB model is now used widely in modern hydrodynamic simulations.

6.5.1 *Derivation of SNB Model*

The basic equations for deriving SNB model is the same as (6.17) except for the collision operator. Assuming scattering frequency without energy change ν_{ei} and electron-electron thermalize frequency ν_{ee}, the 0th and 1st moment equation to the angle μ are derived as follows [17, 18].

$$\frac{v}{3}\frac{\partial}{\partial x}f_1 - \frac{eE}{3mv^2}\frac{\partial}{\partial v}\left(v^2 f_1\right) = -2\nu_{ee}\left(f_0 - f_0^M\right) \tag{6.76}$$

$$v\frac{\partial}{\partial x}f_0 - \frac{eE}{m}\frac{\partial}{\partial v}f_0 = -\nu_{ei}f_1 \tag{6.77}$$

Different from SH derivation, SNB model assumes the following form to the electron distribution function.

$$\begin{aligned} f_0 &= f_0^M + \delta f_0 \\ f_1 &= f_1^M + \delta f_1 \end{aligned} \tag{6.78}$$

The SH has assumed $\delta f_0 = 0$ and $\delta f_1 = 0$. In order to include the flux limit and non-local preheating effects, SNB model derives new equations to obtain the perturbations for δf_0 and δf_1 with reasonable assumption. Since the ${f_1}^{\mathrm{M}}$ in (6.78) is defined by (6.18), a relation to δf_0 and δf_1 from (6.77) is derived to be.

$$v\frac{\partial}{\partial x}\delta f_0 - \frac{eE}{m}\frac{\partial}{\partial v}\delta f_0 = -\nu_{ei}\delta f_1 \tag{6.79}$$

where E is given by the SH relation (6.21) and by including the density gradient it is give as

$$E = \frac{T_e}{n_e}\frac{\partial n_e}{\partial x} + \gamma\frac{\partial T_e}{\partial x} \tag{6.80}$$

where the coefficient g is a function of the ion charge Z in the form [15].

$$\gamma = 1 + \frac{3(Z + 0.477)}{2(Z + 2.15)} \tag{6.81}$$

The Z-dependence is derived due to the change of ration between ion and electrons in the scattering coefficient ν_{ei} in (6.77).

Define the two mean-free paths for an electron with velocity v in the form.

$$\lambda_{ee} = \frac{v}{\nu_{ee}}, \quad \lambda_{ei} = \frac{v}{\nu_{ei}} \tag{6.82}$$

SNB strategy is to delete the velocity derivative term with an intuitive way. It is clear that the second term at LHS in (6.79) is the acceleration or deceleration by electric field. The high energy electrons are decelerated by the ambipolar electric field E and the return current electrons are accelerated. Since the dynamics of the high-energy electrons is important in the transport modeling, the second term works as an deceleration and it can be modeled as the increase of the collision frequency as [15].

$$\frac{1}{\lambda_{ei}^{(E)}} = \frac{1}{\lambda_{ei}} + \left|\frac{eE}{1/2mv^2}\right| \tag{6.83}$$

Note that (6.83) is not appropriate if the E-field dominantly accelerate electron. In SNB model, the deceleration of high-energy component limiting the heat flux is mainly taken account with (6.83). Equation (6.79) is reduced to the following form.

$$\lambda_{ei}^{(E)}\frac{\partial}{\partial x}\delta f_0 + \delta f_1 = 0 \tag{6.84}$$

In SH derivation, only the relation (6.77) is used to derive the f_1 as in (6.18). However, we have to solve (6.76) at the same time as the second relation for δf_0

and δf_1. In addition, as is explained later, the return current effect is neglected in the formulation and (6.76) is modified to the following relation;

$$\delta f_0 + \frac{\lambda_{ee}}{6}\frac{\partial}{\partial x}\delta f_1 = -\frac{\lambda_{ee}}{6}\frac{\partial}{\partial x}g_1^M \tag{6.85}$$

The function g_1^M is a modified form of f_1^M to be explained later. Inserting (6.84) into (6.85), it is easy to obtain δf_0 *and* δf_1 numerically.

In order to know qualitative property of the solutions, discuss about the case with constant mean free paths in space. Then, (6.85) is written in a form;

$$\begin{aligned} &\frac{\partial^2}{\partial x^2}\delta f_0 - \frac{1}{\lambda^2}\delta f_0 = S(x,v) \\ &S(v,x) = -\lambda_{ei}^{(E)}\frac{\partial}{\partial x}g_1^M \\ &\lambda = \sqrt{\frac{\lambda_{ee}\lambda_{ei}^{(E)}}{6}} \end{aligned} \tag{6.86}$$

where the source term S is a function of x for a given velocity v in the form and we introduced an effective mean free path λ(v). It is easy to formally solve (6.86) in the form.

$$\delta f_0(x,v) = \frac{\lambda(v)}{2}\int_{-\infty}^{\infty} S(x',v)\, exp\left(-\frac{|x-x'|}{\lambda(v)}\right)dx' \tag{6.87}$$

Let us consider how flux limit and nonlocal preheat are modeled in this SNB transport model. As seen in Fig. 6.6, the flux limit appears when the mean free path becomes long to approach the temperature gradient scale, namely λ/L_T becomes of the order of unity. Let us assume that this condition means the first term becomes larger than the second term in LHS of (6.86). In such condition, we can obtain the following approximate relation from (6.85).

$$\delta f_1 \approx -g_1^M \tag{6.88}$$

As the result, $f_1 \to 0$ to result a strong flux limitation from (6.78).

On the other hand, the opposite condition $\lambda/L_T >> 1$ is satisfied especially for the high energy component of electrons. Such component has long mean free path in (6.86) and the hear flux from the heating region propagates to the heat front region.

6.5.2 Multi-group Heat Flux

In SNB model, the heat flux is defined as a sum of multi-group heat fluxes. Let us see the definition of the heat flux by the velocity component (v_{g-1}, v_g), where g is an integer of each group of velocity. Each group g also corresponds to the normalized energy group β_g, where $\beta = mv^2/T_e$.

Since the effect of electric field to prevent the heat flux is taken into account as (6.83), the electric field in (6.18) is neglected and the form (6.30) is more simplified as

$$f_1^M = \frac{\lambda_c(\beta = 1)}{L_T}\beta^2(\beta - 4)f_0^M \tag{6.89}$$

$$\rightarrow g_1^M = \frac{\lambda_c(\beta = 1)}{L_T}\beta^2 f_0^M \tag{6.90}$$

In SNB model, the total heat flux q_e^{SNB} is given as the sum of N groups due to g_1^M and δf_1

$$q_e^{SNB} = \sum_{i=1}^{N} Q_1^i + Q_2^i \tag{6.91}$$

where

$$Q_1^i = \frac{2\pi m}{3}\int_{v_{i-1}}^{v_i} g_1^M v^5 dv \tag{6.92}$$

$$Q_2^i = \frac{2\pi m}{3}\int_{v_{i-1}}^{v_i} \delta f_1 v^5 dv \tag{6.93}$$

Note that the first term is written also as

$$Q_1^i = q_e^{SH}\frac{1}{24}\int_{\beta_{i-1}}^{\beta_i} \beta^4 e^{-\beta} d\beta \;\; \Rightarrow \sum Q_1^i = q_e^{SH} \tag{6.94}$$

The total flux is given by Spitzer-Harm heat flux (6.25) and 1/24 is the normalization factor. By replacing f_1^M with g_1^M, the total heat flux is the same as Spitzer-Harm one, while the maximum in the integral of (6.94) becomes $\beta = 4$. This means the mean free path of electrons carrying the maximum heat is $\lambda = 32\lambda_e$, the recommended value for the LMV model [11].

It should be noted that Q_2^i modify the heat flux due to the electron components with long mean free path as can be guess from the propagator form. This term reduces the heat flux as flux limiter and provides heat flux by electrons of long mean free path, namely pre-heating is given by this new term.

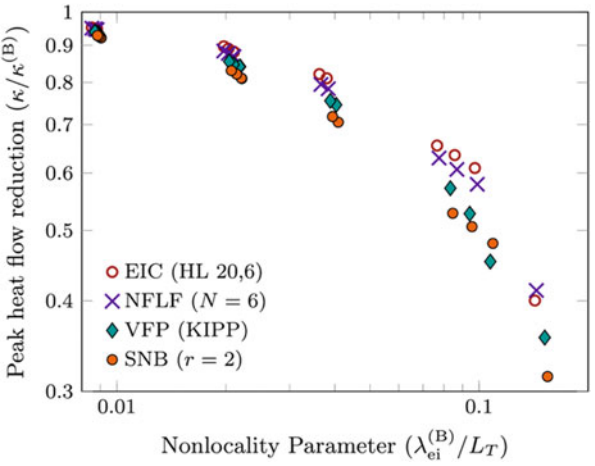

Fig. 6.12 Flux limitation property is compared among three models and VFP simulation with KIPP code. This is the same plot as Fig. 6.6, but for more realistic temperature profile. All three models show good agreement as VFP simulation result. The heat flux is limited dramatically for the case where the temperature gradient scale L_T approached to ten times the electron scattering mean-free-path. Reprint with permission from Ref. [19]. Copyright 1998 by American Institute of Physics

Fourier spectrum of the transport propagator shown in Fig. 6.7 is calculated for SNB model and other models. They are compared in Fig. 6.12 to the other numerical models [18]. The results of VFP code KIPP is shown. Compared to the VFP result, the simple SNB model is found to reproduce the result well. The other data are explained in [18]. Considering the computation time, the SNB is very convenient, especially modeling the effect of flux limit and preheating in hydrodynamic simulation code. Note that r = 2 is a coefficient of modeling electron-electron collision which is approximated with a simple form in (6.76). It is reported that using BGK collision operator with r = 2 gives a good agreement with VFP calculation.

The multi-group diffusion model "SNB model" is widely used in several ICF codes such as Lawrence Livermore National Laboratory's HYDRA, CELIA laboratory's CHIC, CEA's FCI2, DUED (U. Rome), and the University of Rochester Laboratory for Laser Energetics' LILAC and DRACO [18]. It is also applicable to multi-dimensional space codes with magnetic fields [19].

Transport codes are compared in the background hydrodynamics obtained with HYDRA code. Gadolinium hohlraum containing a typical helium gas is heated by laser and the density and temperature profile at t = 20 ns are used as the initial condition of each code. After 5 ps run of simulation codes, the heat flux profiles are plotted in Fig. 6.13 [18]. In Fig. 6.13, "Local" is the heat flux calculated with Braginskii formula, which is equivalent to Spitzer-Harm heat flux. Two models of SNB are shown. It is clear that the SNB model provides well the property of flux limitation near the heating region and preheating character near the heat front as predicted by VFP simulation code IMPACT.

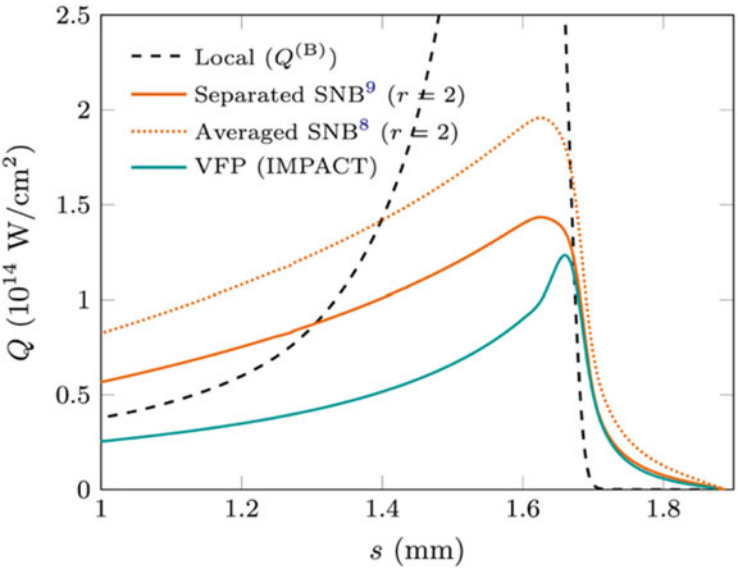

Fig. 6.13 Heat flux distribution near the ablation front of high-Z material. VFP simulation result is shown with green line. It is typical that the maximum of heat flux is limited and the preheating tail is given. The SH extremely over-estimates the heat flux as shown in the dashed line. The model SNB with multi-group is more reasonable and the flux limitation and preheating are well modeled. Reprint with permission from Ref. [19]. Copyright 1998 by American Institute of Physics

6.6 Comparison of SNB Model to Two Different Experiments

By use of Thomson scattering diagnostics, electron distribution functions are measured in a model experiment of aluminum plasma ablating into the vacuum. An aluminum foil is irradiated with six beams 3ω laser with 2 ns pulse width and for the diagnostic probe 2ω laser is used [20]. The five points of ablating plasma are measured for Thomson scattering. In the present case, the scattered spectral shape is used to determine the electron distribution function at each point. The measured electron temperature and density are 1 ~ 1.3 keV and 0.5 ~ 1x10^{20} cm^{-3}, respectively. Speculated density scale lengths are in the range $\lambda_{ei}/L_T = 1.4 \times 10^{-2} \sim 7 \times 10^{-3}$.

In the analysis of Thomson scattering data, the following spectral density function S(**k**,ω) of electron plasma contribution is used at high frequency region, where the ion contribution can be neglected. Note that the previous experiment in Chap. 6.4 has used only the ion acoustic wave contribution in low frequency region, and therefore only the information of electron temperature is inferred from Thomson data. The spectral density function by electron plasma is given as [21].

$$S(\boldsymbol{k},\omega) = \frac{2\pi}{k}\frac{f_e(\omega/\boldsymbol{k})}{|\epsilon(\boldsymbol{k},\omega)|^2} \tag{6.95}$$

where $f_e(\omega/\boldsymbol{k})$ is the one-dimensional electron distribution function and $\epsilon(\boldsymbol{k},\omega)$ is the dielectric constant of electron plasma wave.

The Thomson scattering is dominated by the contribution of the plasma waves satisfying the dispersion relation (resonance condition),

$$\epsilon(\boldsymbol{k},\omega) = 0 \quad \Rightarrow \quad \omega(k) = \pm\omega_L(k) + i\gamma_L(k) \tag{6.96}$$

The electron plasma wave is called Langmuir wave with the frequency $\omega_L(k)$. In general, the resonance solution is complex as in (6.96) and the imaginary part $\gamma_L(k)$ is due to wave damping by Landau damping process. It is well known that the **Landau damping** is proportional to a velocity derivative at the resonance speed, $\gamma_L(k) \propto \partial f_e/\partial v$ at $\mathrm{v} = \omega_\mathrm{L}/\mathrm{k}$. By use of these theoretical relations and compare them to Thomson scattering spectra, it is possible to obtain the local electron distribution function in non-Maxwell form. This data also provides the electron density and temperature values at the scattered five points in the experiment.

In Fig. 6.14, the resultant heat flux obtained by the **Thomson scattering** data (TS) is shown with red circles (The detail of TS principle will be discussed in Chap. 9). Spitzer-Harm heat flux is also shown with use of the temperature distribution at the five points as (SH) with blue triangles. In order to check the validity of the nonlocal transport model SNB described in the previous section, a multi-group simulation code has been used for the density and temperature profiles obtained in the experiment. The SNB result is shown with black diamonds. The authors insists that SNB nonlocal transport model cannot reproduce the experimental data and it is about the halfway between SH and the experimental heat flux. I think this concluding remark is too strict for evaluating a robust nonlocal transport model such as SNB. As we have studied in the previous section, SNB guarantees the preheating and flux limit physics, while it is not so strict theoretical model to compare the form of distribution functions.

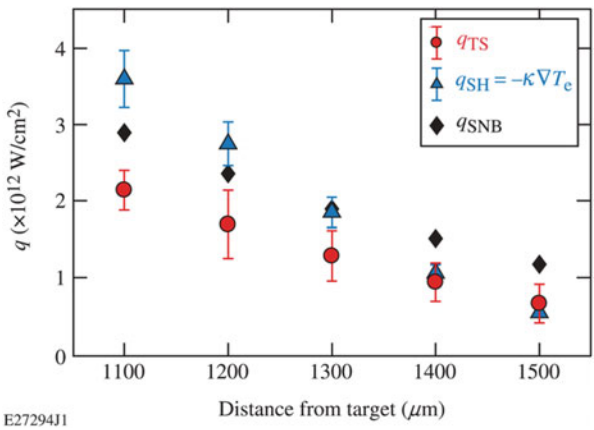

Fig. 6.14 The heat flux observed experimentally is compared to those from SH diffusion and SNB transport models. Reprint with permission from Ref. [21]. Copyright 1998 by American Physical Society

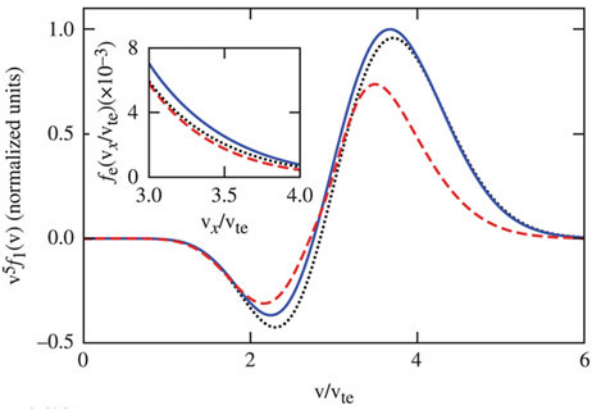

Fig. 6.15 Comparison of the velocity dependent heat flux at the point in the experiment. Three curves are from FP calculation (dashed red curve), Spitzer-Harm (solid blue curve), and SNB (dotted black curve). Reprint with permission from ref. [21]. Copyright 1998 by American Physical Society

It is also informative to show Fig. 6.15 [20]. The velocity dependent heat flux (6.22) is plotted for one point (1200 μm). Three curves are from FP calculation (dashed red curve), Spitzer-Harm (solid blue curve), and SNB (dotted black curve). It is not so meaningful to compare the distribution function of heat flux. Since the introduction of the function g_1^M instead of Spitzer-Harm f_1^M in (5.15) has no mathematical base and just to avoid too much negative component. So, in general there may be other ways to replace f_1^M to a convenient way for modeling nonlocal transport. The reason why g_1^M is introduced is that it guarantees the preheating effect and the property of flux limit robustly.

It is difficult to say, therefore, that there is not seen an improvement of heat flux in SNB model because it is almost the same as SH, but different from FP result. The validity of SNB should be checked under the condition that the heat flux is strongly inhibited like the flux limit and in the opposite case that the high energy electrons penetrate into cold plasma region. In addition, it is noted that SNB requires to be adjusted about the collisional modeling.

The preheating has been studied in relatively higher density plasma comparing to the experimental data of plastic form plasma with the density near 0.1 g/cm^3 and temperature near 30 eV [22]. As a tool to study such high-density plasma, so-called warm dense matter (WDM), the authors used X-ray Thomson scattering diagnostic to obtain the electron temperature, density, and ionization state by comparing x-ray spectrum with theoretical one, by varying the plasma parameters. The target is made of plastic, gold, aluminum and plastic form layers to observe the preheating effect in the plastic form layer.

In the experiment, preheating of the expanding form plasma was observed and a variety of simulations have been carried out to find the physical source to give preheating to the form region over the high-density plasma region. Even with detail opacity and radiation transport, it was not possible to obtain enough preheating energy flux to the form region. It was finally concluded that about 10% of the free streaming heat flux from the shocked high-density region transfers large amount of heat to preheat the preheat region more than 30 eV as shown in Fig. 6.16 [22]. It is

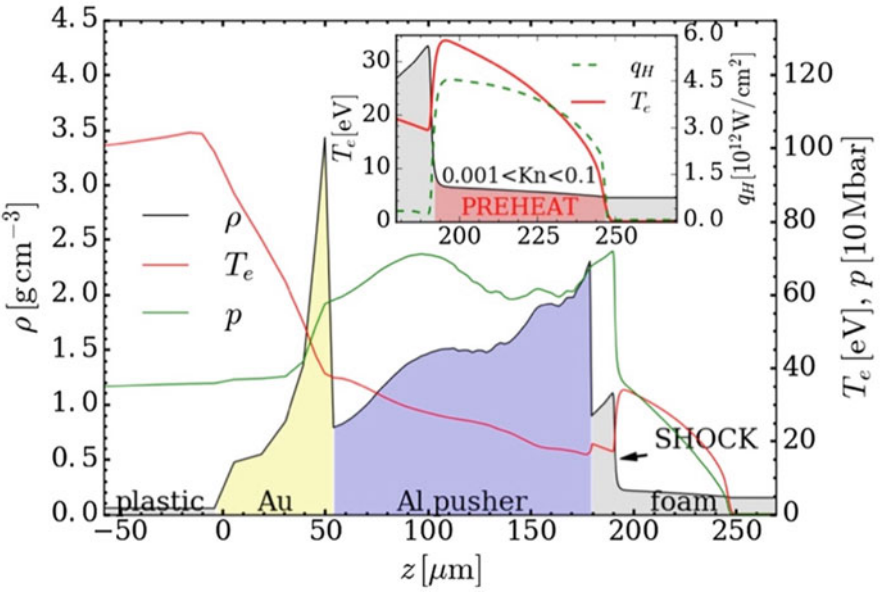

Fig. 6.16 A multi-layered target is heated by laser to find the preheating in the rear side of the target. The enhanced temperature has been measured as preheat in CH foam region in the experiment and computationally reproduced by including non-local transport model. Reprint with permission from Ref. [22]. Copyright 1998 by American Physical Society

surprising to know that the temperature of preheating region is higher than the upstreaming region of the heat flux. It is unphysical in the local thermodynamic equilibrium (LTE) thermodynamics. There should be some unknown physics at the shock front, where the temperature decreases from the front to the rear of the shock front, this means an entropy of plasma decreases by the shock wave. It is not clear why such result is obtained in a nonlocal simulation, while one thing to be clarify is that the contribution of electrostatic field at the shock surface.

As explained in modeling nonlocal transport, it is hard to model the effect of electrostatic field even n one-dimensional system. In SNB model, the electric field is included into an effective mean free path as shown in (6.83) and the electric field is evaluated from the neutral current condition (6.21). Note that there is no density gradient dependence and the force to electrons -eE is the direction of – dT_e/dx. However, the electrostatic field at the shock front is in general given by the Boltzmann relation;

$$n_e(x) = n_0 \, exp\left[e\frac{\phi(x)}{T_e}\right] \quad \Rightarrow \quad e\phi_{01} = T_e \, ln\left(\frac{n_0}{n_1}\right) \tag{6.97}$$

The potential jump at the shock front is more than Te (~20–30 eV) and most of the electrons with energy more than $e\phi_{01}$ are reflected back at the shock front. The evaluation of E field in any non-local transport is difficult issue.

Appendix-C. Fokker-Planck Equation

Vlasov equation is a powerful equation in studying waves, transport, turbulence, and so on from view point of wave-particle interaction and non-Maxwellian plasmas. As mentioned already, Vlasov equation is applicable only for collisionless physics in plasmas. However, collisional effect cannot be neglected in some non-LTE plasmas, especially plasma with strong heat flow and inhomogeneity of physical quantities. Principally, of course, it is required to solve Boltzmann equation of (C.1) with appropriate collision cross section. It is, however, not so easy to solve such differential-integral equation directly. Such collision effect in plasmas is the same as random walk or thermal noise widely seen in the nature. It is easy to use **Fokker-Planck equation** used widely in non-equilibrium statistical mechanics.

Langevin to Fokker-Planck Equation

In order to clarify the intuitive image of the readers to Fokker-Planck equation, it is better to start with a simple one-dimensional **Langevin equation** for a Brownian motion in spatially uniform medium.

$$m\frac{dV(t)}{dt} = -\nu_f mV(t) + mR(t) \tag{C.1}$$

Here the 1st term in RHS is the frictional force and the 2nd term is a random force。 Such equation is called **stochastic differential equation**. The governing equation to the velocity distribution function P(v,t) defined as ensemble average probability distribution in velocity space is given as follows as will be explained from now.

The ensemble average of any physical quantity of function V is defined by

$$\langle A(V)\rangle = \int_{-\infty}^{\infty} A(v)P(v,t)dv \tag{C.2}$$

The random force R(t) in (C.1) is Markovian process with Gaussian probability to given as

$$\langle R(t)\rangle = 0, \quad \langle R(t)R(t')\rangle = D\delta(t-t') \tag{C.3}$$

and the following relation is satisfied.

$$\Delta W = \int_{t}^{t+\Delta t} R(t)dt \tag{C.4}$$

$$\langle \Delta W \rangle = 0 \tag{C.5}$$

$$\langle \Delta W^2 \rangle = D\Delta t \tag{C.6}$$

Expanding A(V) with Taylor series in velocity, the following relation is obtained

$$A(V(t+\Delta t)) = A(V(t)) + \left.\frac{dA}{dV}\right|_{V=V(t)} \Delta V(t) + \frac{1}{2}\left.\frac{d^2A}{dV^2}\right|_{V=V(t)} \Delta V(t)^2 + \cdots \tag{C.7}$$

Taking the ensemble average of (C.7) yields the following form

$$\langle A(V(t+\Delta t))\rangle = \langle A(V(t))\rangle + \left\langle \left.\frac{dA}{dV}\right|_{V=V(t)} \Delta V(t) \right\rangle + \frac{1}{2} \times \left\langle \left.\frac{d^2A}{dV^2}\right|_{V=V(t)} \Delta V(t)^2 \right\rangle + \cdots \tag{C.8}$$

Taking finite difference of (C.1) and inserting ΔV(t) in (C.8) and keeping the term proportional only to the 1st order of Δt, the following equation can be derived finally.

$$\frac{d}{dt}\langle A(V(t))\rangle = -\nu_f \left\langle V(t)\frac{dA}{dV}\right\rangle + \frac{D}{2}\left\langle \frac{d^2A}{dV^2}\right\rangle \tag{C.9}$$

It is noted that the second term of RHS of (C.9) is remains as the 1st order because of (C.6).

Return to the definition (C.2), (C.9) can be changed to the equation to probability function P(v,t) as follows. The LHS of (C.9) is

$$\frac{d}{dt}\langle A(V(t))\rangle = \int_{-\infty}^{\infty} A(v)\frac{\partial P(v,t)}{\partial t}dv \tag{C.10}$$

The 1st term of RHS of (C.9) is

$$-\nu_f \left\langle V(t)\frac{dA}{dV}\right\rangle = -\nu_f \int_{-\infty}^{\infty} v\frac{dA}{dv}P(v,t)dv = \nu_f \int_{-\infty}^{\infty} A(v)\frac{\partial}{\partial v}\{vP(v,t)\}dv \tag{C.11}$$

Where partial integral is used with the assumption that $P(\infty,t) = P(-\infty,t) = 0$.

$$\left\langle \frac{d^2A}{dV^2}\right\rangle = \int_{-\infty}^{\infty} \frac{d^2A(v)}{dv^2}P(v,t)dv = \int_{-\infty}^{\infty} A(v)\frac{\partial^2 P(v,t)}{\partial v^2}dv \tag{C.12}$$

The 2nd term of RHS is modified by using the partial difference two times. As the result, (C.9) should be satisfied for any function A(v) only when the condition:

$$\frac{\partial P(v,t)}{\partial t} = \nu_f \frac{\partial}{\partial v}[vP(v,t)] + \frac{D}{2}\frac{\partial^2 P(v,t)}{\partial v^2} \tag{C.13}$$

is satisfied. (C.6) is Fokker-Planck equation.

It should be noted that solving Fokker-Planck equation is exactly the same as calculating an ensemble average for many test particles motioned by Langevin Eq. (C.1). As a simple examples, Fokker-Planck equation is used to study any Brownian motion, white noise in electric circuit, polymer dynamics, etc.

It is useful think about the case of stationary state of (C.13). Then, RHS of (C.13) should vanish and the following relation should be satisfied after integrating it:

$$\frac{dP(v)}{dv} = -\frac{2\nu_f}{D} vP(v) \tag{C.14}$$

This can be easily solved to give

$$P(v) = exp\left(-\frac{\nu_f}{D}v^2\right) \tag{C.15}$$

This is the velocity distribution in the equilibrium state and should be Maxwellian distribution, namely the diffusion coefficient in velocity space given in (C.13) should satisfy the following condition.

$$\frac{D}{2} = \frac{T}{m}\nu_f \tag{C.16}$$

It is very interesting to compare the diffusion coefficient in velocity space (C.16) and that in real space (5.71) which is called Einstein relation. Note that dependence on the collision frequency is opposite. In a very collisional system, the diffusion in velocity space is fast and get to be equilibrium soon, while in the real space it is very slow to diffuse.

In plasmas, collision frequency is a strong function of the particle velocity and in non-LTE plasmas the distribution function is not isotropic in 3-dimensional velocity space. It is, therefore, difficult to directly use Fokker-Planck equation of (C.13). It is now easier, however, to extend the above mathematical derivation from Langevin equation to Fokker-Planck equation. Then, it is clear that the following Fokker-Planck equation can be obtained in 3-diemnsional space of velocity.

$$\frac{\partial P(\boldsymbol{v},t)}{\partial t} = \frac{\partial}{\partial v_i}\left[\left\langle\frac{\Delta v_i}{\Delta t}\right\rangle P(\boldsymbol{v},t)\right] + \frac{1}{2}\frac{\partial^2}{\partial v_i \partial v_j}\left[\left\langle\frac{\Delta v_i \Delta v_j}{\Delta t}\right\rangle P(\boldsymbol{v},t)\right] \tag{C.17}$$

This expression is easily understood that RHS of (C.17) is an extension to 3 dimension of Taylor expansion and the form is derived with the same manner as (C.8), (C.9), and (C.10).

What Fokker-Planck equation says is that any random force in Brownian motion reduces to the combination of the friction term and diffusion term.

It is noted that the probability function P(**v**,t) in (C.17) is the ensemble averaged velocity distribution function in velocity space and it is exactly the same as the velocity distribution function at each real space point as long as the collision is taken place at a point and no change in **r** after each binary collision.

After a long algebra shown in [5], new functions and constant are introduced

$$\Gamma = \frac{Z^2 e^4}{4\pi\varepsilon_0^2 m^2} \ln\Lambda \tag{C.18}$$

$$H(\boldsymbol{v}) = Z_s^2 \left(\frac{m+m_s}{m_s}\right) \int \frac{f_s(\boldsymbol{v}_s)}{g} d\boldsymbol{v}_s \tag{C.19}$$

$$G(\boldsymbol{v}) = Z_s^2 \int \mathrm{g} f_s(\boldsymbol{v}_s) d\boldsymbol{v}_s \tag{C.20}$$

Here g is a function of **v** and $\mathbf{v}_s$ and given in [5]. It is noted that the definition (C.19) and (C.20) are called the **Rosenbluth potentials**. It is well known that the Fokker-Planck equation is reduced to the following form.

$$\left(\frac{\partial}{\partial t} f\right)_{coll} = -\Gamma \frac{\partial}{\partial v_k}\left(\frac{\partial H}{\partial v_k} f\right) + \frac{1}{2}\Gamma \frac{\partial^2}{\partial v_k \partial v_j}\left(\frac{\partial^2 G}{\partial v_k \partial v_j} f\right) \tag{C.21}$$

It is known that the first term of RHS in (C.21) is the dynamical friction and the second one is the diffusion term. The Fokker-Planck equation assumes only the scattering by the binary Coulomb collision, therefore, in the system of two kind of particles like fully-ionized ions and electrons, we have to solve the equation for electron distribution function changing in time by scattering electron-electron(e-e), electron-ion(e-i) and for ion distribution by ion-electron(i-e), ion-ion(i-i). It is noted that in the case of e-e and i-i scattering, (C.7) is a nonlinear equations to the distribution function.

In order to see what happens to a test particle injected from the boundary due to the Coulomb collision in a uniform plasmas, assume the distribution function of the particle is a delta function.

$$f(\boldsymbol{v}, t) = \delta\{\boldsymbol{v} - \boldsymbol{u}(t)\} \tag{C.22}$$

Inserting (C.22) to (C.21) and taking the **v** moment of (C.21) lead the following simple form.

$$\frac{\partial \boldsymbol{u}(t)}{\partial t} = \Gamma \frac{\partial H(\boldsymbol{u})}{\partial \boldsymbol{u}} = -\nu_f(u)\boldsymbol{u} \tag{C.23}$$

The term with G vanish in partial integral process. Equation (C.23) clearly shows that the term H gives the drag force and the frictional coefficient ν_f is calculated. Fokker-Planck equation is more precise equations for the ion stopping discussed in Sect. 4.8. In ion stopping simulation, however, the ionization process should be also included in RHS of (C.21).

Fokker-Planck Equation in Maxwellian Scatterers

It is useful to show the explicit form of Fokker-Planck equation of (C.21) in the case of the distribution of the scatterers is Maxwellian with temperature T_s and mass m_s.

$$f_s(\boldsymbol{v}_s) = f_M(v_s) = n_s \frac{a_s^3}{(\pi)^{3/2}} exp\left(-a_s^2 v_s^2\right) \tag{C.24}$$

$$a_s^2 = \frac{m_s}{2T_s} \tag{C.25}$$

Here n_s are the number density of the scatterers.

$$x = a_s v \tag{C.26}$$

$$\int_{-\infty}^{\infty} \frac{e^{-y^2}}{|\boldsymbol{y} - \boldsymbol{x}|} d^3\boldsymbol{y} = \frac{\pi^{3/2}}{x} erf(x) \tag{C.27}$$

The Rosenbluth potentials is given in the flowing form by use of the spherical symmetry in velocity space.

$$\begin{aligned} &erf(x) = \frac{2}{\sqrt{\pi}} \int_0^x e^{-y^2} dy, \\ &erf(x) = 1 \quad (x \to \infty), \quad erf(x) = \frac{2}{\sqrt{\pi}} x \quad (x \to 0) \end{aligned} \tag{C.28}$$

Here erf(x) is an error function defined as

$$H(v) = Z_s^2 \left(\frac{m + m_s}{m_s}\right) a_s n_s \pi^{3/2} \frac{erf(x)}{x} \tag{C.29}$$

The G defined in (C.20) reduces

$$G(v) = \frac{Z_s^2 n_s}{2a_s} \left[\frac{d}{dx} erf(x) + \left(\frac{1}{x} + 2x\right) erf(x)\right] \tag{C.30}$$

It should be noted that since the Maxwell distribution is isotropic in velocity space and depend only on the absolute value of the velocity, H and G reduce to functions only on v as shown in (C.29) and (C.30).

If the distribution function of the scatterers is isotropic in the velocity space, H and G can be given only functions of v. Therefore, the following convenient relations can be obtained.

$$\frac{\partial H}{\partial v_k} = \frac{\partial v}{\partial v_k}\frac{\partial H}{\partial v} = \frac{dH}{dv}\frac{\partial v}{\partial v_k} \tag{C.31}$$

and

$$\frac{\partial^2 G}{\partial v_k \partial v_j} = \frac{\partial^2 G}{\partial v^2} = \frac{d^2 G}{dv^2} \tag{C.32}$$

The v derivative of H and G in (C.31) and (C.32) can be obtained explicitly as

$$\frac{d}{dx}\left(\frac{erf(x)}{x}\right) = -\frac{1}{x^2}erf(x) + \frac{2}{\sqrt{\pi}x}e^{-x^2} = 2\psi(x) \tag{C.33}$$

$$\frac{d^2}{dx^2}\left[\frac{derf(x)}{dx} + \left(\frac{1}{x} + 2x\right)erf(x)\right] = \frac{2}{x^3}\left[erf(x) - \frac{2x}{\sqrt{\pi}}e^{-x^2}\right] = \frac{4}{x}\psi(x) \tag{C.34}$$

Here Ψ(x) is defined as

$$\psi(x) = \frac{1}{2x^2}\left[erf(x) - \frac{2x}{\sqrt{\pi}}e^{-x^2}\right] \tag{C.35}$$

References

1. L. Spitzer, R. Harm, Heat conduction of an electron gas. Phys. Rev. **89**, 977 (1953)
2. R.C. Malone, R.L. MaCrory, R.L. Morse, Indications of strongly flux-limited electron thermal conduction in laser-target experiments. Phys. Rev. Lett **34**, 721 (1975).: Craxton et al., Direct-drive inertial confinement fusion: A review, Phys. Plasmas 22, 110501, Chap. 11 (2015)
3. E.M. Eppeliene, R.W. Short, A practical nonlocal model for electron heat transport in laser plasmas. Phys. Fluids B **3**, 3092 (1991)
4. T.A. Mehlohrn, J.J. Duderstadt, A discrete ordinates solution of the Fokker-Planck equation characterizing charged particle transport. J. Comp. Phys. **38**, 86 (1980)
5. T.J.M. Boyd, J.J. Sanderson, *The Physics of Plasmas* (Cambridge University Press, 2003). Chap. 8
6. M.N. Rosenbluth, W.M. MacDonald, D.L. Judd, Fokker-Planck equation for an inverse-square force. Phys. Rev. **107**, 1 (1957)

7. A.R. Bell, R.G. Evans, D.J. Nicholas, Electron energy transport in steep temperature gradients in laser-produced plasmas. Phys. Rev. Lett. **46**, 243 (1981)
8. A.R. Bell, Non-Spitzer heat flow in a steadily ablating laser-produced plasma. Phys. Fluids **28**, 2007 (1985)
9. J.R. Albriton, Laser absorption and heat transport by non-Maxwell-Boltzmann electron distributions. Phys. Rev. Lett. **50**, 2078 (1983)
10. E.M. Epperlein, Kinetic theory of laser filamentation in plasmas. Phys. Rev. Letts **65**, 2145 (1990)
11. J.F. Luciani, P. Mora, J. Virmont, Nonlocal heat transport due to steep temperature gradients. Phys. Rev. Lett. **51**, 1664 (1983)
12. J.R. Albriton et al., Nonlocal electron heat transport by not quite Maxwell-Boltzmann distributions. Phys. Rev. Lett. **57**, 1887 (1986)
13. G. Gregori et al., Effect of nonlocal transport on heat-wave propagation. Phys. Rev. Lett. **92**, 205006 (2004)
14. V.Y. Bychenkov et al., Nonlocal electron transport in a plasma. Phys. Rev. Lett. **75**, 4405 (1995)
15. G.P. Schurtz, P.D. Nicolai, M. Busquet, A nonlocal electron conduction model for multidimensional radiation hydrodynamics codes. Phys. Plasmas **7**, 4238 (2000)
16. M. Sherlock, J.P. Brodrick, C.P. Ridgers, Testing nonlocal models of electron thermal conduction for magnetic and inertial confinement fusion applications. Phys. Plasmas **24**, 082706 (2017)
17. A. Marocchino et al., Comparison for non-local hydrodynamic thermal conduction models. Phys. Plasmas **20**, 022702 (2013)
18. J.P. Brodrick et al., Testing nonlocal models of electron thermal conduction for magnetic and inertial confinement fusion applications. Phys. Plasmas **24**, 092309 (2017)
19. P.D. Nicolai, J.-L.A. Feugeas, G.P. Shultz, A practical nonlocal model for heat transport in magnetized laser plasmas. Phys. Plasmas. **13**, 032701 (2006)
20. R.J. Henchen et al., Observation of nonlocal heat flux using Thomson scattering. Phys. Rev. Letts. **121**, 125001 (2018)
21. D.H. Froula, S.H. Glenzer, N.C. Luhmann Jr., J. Sheffield, *Plasma Scattering of Electromagnetic Radiation: Theory and Measurement Techniques*, 2nd edn. (Academic, Amsterdam, 2011).; S. H. Glenzer and R. Redmer, X-ray Thomson scattering in high energy density plasmas, Rev. Mod. Phys. 81, 1625 (2009)
22. K. Falk et al., Measurement of preheat due to nonlocal electron transport in warm dense matter. Phys. Rev. Lett. **120**, 025002 (2018)